

## Understanding the mechanism of aluminium nanoparticle oxidation

A. RAI, K. PARK, L. ZHOU and M. R. ZACHARIAH\*

Department of Mechanical Engineering and Department of Chemistry and Biochemistry,  
University of Maryland, College Park, MD, USA

(Received 29 July 2005; in final form 11 April 2006)

Aluminium nanoparticles have gained importance in the last decade because of their increased reactivity as compared with traditional micron-sized particle. The physics of burning of aluminium nanoparticle is expected to be different than that of micron-sized particles, and the current article is motivated by these differences. We have previously measured the size resolved reactivity of nanoaluminium by single-particle mass spectrometry, to which we now add transmission electron microscope (TEM) and an on-line density measurement. The latter two studies revealed the presence of hollow particles following oxidation of nanoaluminium and indicating the significance of diffusion of aluminium in the overall process. Based on experimental evidence, we believe that aluminium nanoparticle oxidation occurs in two regimes. Prior to melting of aluminium slow oxidation occurs through the diffusion of oxygen through the aluminium oxide shell. Above the melting point, we transition to a fast oxidation regime whereby both aluminium and oxygen diffuse through the oxide shell to enhance the oxidation rate.

We also develop a phenomenological model for nanoaluminium oxidation that accounts for the experimentally observed rates, the fact that both fuel and oxidizer are diffusing, and a new effect related to internal pressure gradients. The latter phenomenon is based on molecular dynamic simulations suggesting that there are large pressure gradients present inside these particles, with the aluminium core under a positive pressure and the aluminium oxide shell under a negative pressure. We have considered the effect of these pressure gradients on the oxidation process. A power law relation was obtained ( $t \propto r^{1.6 \pm 0.1}$ ) between the time required for oxidation and particle radius.

**Keywords:** Aluminium nanoparticles; Nanoenergetic materials; Nanoparticles oxidation; Oxidation mechanism

### 1. Introduction

Aluminium, because of its high enthalpy of combustion has been added to propellants and explosives. Because of its extensive use as an energetic material, several research efforts have been directed to understand the mechanism and model the oxidation of aluminium particles. Brzustowski and Glassman [1] suggested that metal combustion would be similar to droplet combustion and can be described using the  $D^2$  law and suggested that aluminium will burn in the vapour phase. Several researchers [2, 3] have improved the model by considering the inward diffusion and condensation of the product on the droplet surface, and included the effect of heat of condensation, thus relaxing the assumptions made in the earlier work. Beckstead and

---

\*Corresponding author. E-mail: mrz@umd.edu

coworkers [4–8] have developed a two-dimensional, unsteady state, evaporation–diffusion–kinetics controlled numerical model to describe the oxidation of aluminium particles. Yetter *et al.* [9, 10] have worked extensively on combustion of aluminium. They have studied the flame structure of aluminium particles reacting in various well-defined oxidizing environments experimentally and computationally, and have confirmed the gas phase oxidation of micron-sized particle. More recently Trunov *et al.* [11] studied the effect of phase transformations in the aluminium oxide shell, which surrounds the metal particle, on the oxidation process. They have considered oxidation to be a transport process through the oxide shell as opposed to the vapour phase phenomenon as was done by most of the earlier researchers and have proposed a multi-stage mechanism for oxidation of micron-sized aluminium powder.

Most of these earlier models described the oxidation of micron-sized aluminium particles and these particles effectively burn in the continuum regime with a boundary layer and a flame surrounding the particle. In this regime the metal burns in the vapour phase and the diffusion flux of the metal from the particle surface, and that of the oxidizer from the ambient atmosphere determine the standoff distance of the flame from the particle surface. The criteria for continuum burning is that the particle size be significantly greater than the mean free path of the gas and is clearly the case for micron size particles. It is well known that fine metal particles (<300 nm) or metal nanoparticles (<100 nm) are highly reactive. It has been reported [12] that addition of aluminium nanoparticles in a propellant formulation can enhance the propellant burning rate by a factor of 5–10 over conventional micron-sized particles. Nanoparticles ( $d < 100$  nm) are typically smaller than the mean free path, and a continuum burning model is not valid. Oxidation of these nanoparticles will likely be more of a surface process involving the collision of oxygen with the particles and then the subsequent transport through the oxide shell. Furthermore there are/maybe other physical/chemical differences between nanoparticles and micron-sized materials.

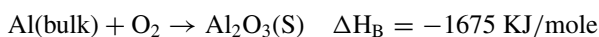
It has been reported [13], using thermogravimetry (TGA) and differential thermal analysis (DTA), that aluminium nanoparticles formed by electrical wire explosion can ignite at a temperature as low as 550°C, considerably lower than the micron-sized counterpart. Aumann *et al.* [14] have shown that the activation energy for combustion of aluminium nanoparticles is smaller than that of a bulk aluminium sample. In our earlier work, we reported [15] on the importance of phase change of aluminium on the oxidation of aluminium nanoparticles and have observed that the onset of oxidation is closely associated with the melting of aluminium, rather than being below it. More recently [16] we employed quantitative single particle mass spectrometry to determine the size resolved kinetic rate constants for aluminium oxidation and confirmed that in the absence of any heat and mass transfer effects, smaller particles are more reactive and that oxidation is preceded by an aluminium phase transformation.

In the current paper we look at the oxidation process from a mechanistic perspective. A better understanding of the mechanism of oxidation of isolated aluminium nanoparticle will help in predicting the combustion behaviour of the energetic formulations in which these particles are added as an additive for enhanced rate of energy release. To understand the oxidation process, the evolving morphology of oxidized aluminium particles was studied using the transmission electron microscope (TEM). We also measured the inherent density of oxidized aluminium particles using a combination of differential mobility analyser (DMA) [17], aerosol particle mass analyser (APM) [18, 19] and TEM. We develop a phenomenological model that incorporates prior results on kinetic measurements [16] as well as some physics unique to these length scales. In the latter case, this involves considering the extremely high internal pressure gradients within nanoparticles [20]. We also discuss how these gradients may be important in changing the overall oxidation rate.

## 2. On the increased reactivity of aluminium nanoparticles: thermodynamics versus kinetics

It is a well-known fact that aluminium nanoparticles are more reactive as compared to conventional micron-sized particles. In principle at least this may result from either thermodynamic, (i.e. higher energy release as the grain size is decreased), or from kinetic factors, (i.e. faster energy release as the grain size decreases). There has been speculation that the increase in relative surface energy or perhaps the formation of strain within the nanoparticle would provide a sufficiently higher enthalpy state so as to alter the amount of energy release significantly above that of a bulk material. In other words there might be more energy available thermodynamically in a nanoparticle.

Consider the maximum energy one could hope to achieve over a bulk material. If we consider combustion of aluminium in oxygen, the enthalpy of combustion of bulk aluminium is about 1675 kJ/mol. Next we consider the smallest possible aluminium particle, i.e. a particle with only one atom. The enthalpy of combustion of an isolated aluminium atom is about 2324 kJ/mol.



In other words the most energy one could expect to gain from aluminium combustion is from an isolated aluminium atom. In that case the enhancement over bulk aluminium is a 39% increase in energy release, and this difference is actually just the enthalpy of vaporization. In other words, we cannot do better than the 39% enhancement. Using the bulk value of the surface energy for aluminium of  $0.8878 \text{ J/m}^2$  at 298 K, this enhancement in energy output is reduced to a factor of only 1.04 by the time the particle size is 1 nm. It can reasonably be concluded then that thermodynamic factors alone cannot explain the differences in the burning rates of aluminium nanoparticles and those of conventional micron sized particles. The differences in combustion properties must lie in the kinetics rather than the thermodynamics. That is the focus of this paper.

## 3. Experimental methods

This study has two main experimental aspects: (a) observe the morphology of the oxidized particles to assist in considering the likely mechanism; (b) measure the inherent density of the nanoparticles at different oxidation temperatures. Aluminium nanoparticles were generated in-house to perform these experiments. A complete schematic of the experimental set-up is shown in figure 1.

For the experimental study, we used aluminium nanoparticles generated using a DC arc discharge method, a schematic of which is shown in figure 1. In this method an arc is ignited between a tungsten electrode (cathode) and 99.99% purity aluminium pellets (anode), to evaporate aluminium. A craftsman infinite amperes arc welder was used as a power supply for the arc, which was operated with a voltage of 11–16 V and a current of 30–40 A. Six to seven litres per minute (LPM) of argon was used as a carrier gas to carry the aluminium vapour, while an additional 22–23 LPM of argon was used as quench gas flow to facilitate the condensation of aluminium vapour to form nanoparticles. The DC arc discharge method produces particles with a peak mobility size of 70–80 nm as measured with a DMA [17] and a condensation particle counter (CPC). With this approach particles free of oxygen can be produced and their chemistry studied directly [16, 21].

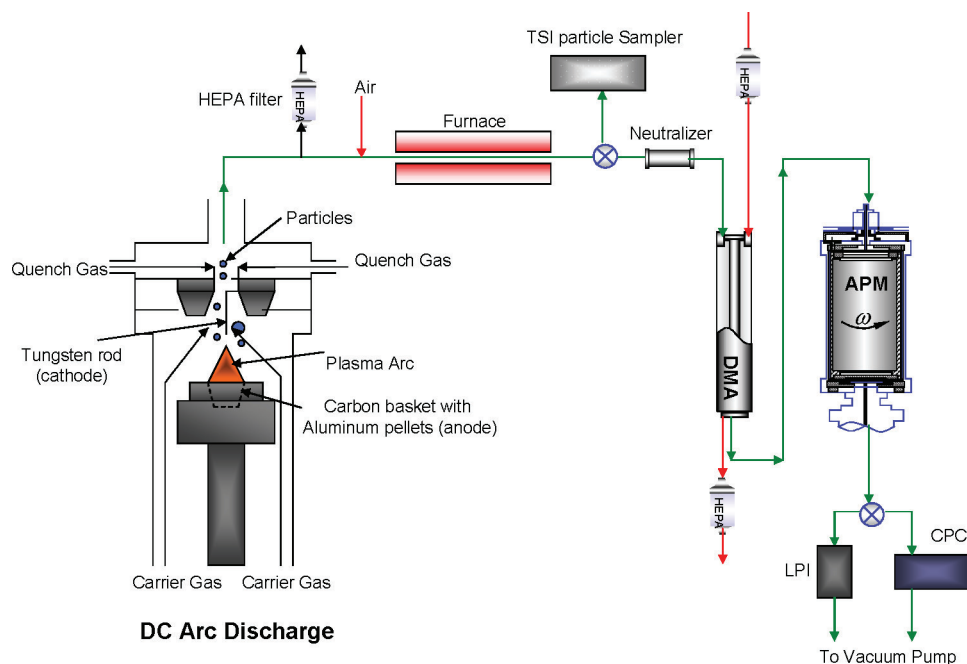


Figure 1. Schematic of the experimental system for density measurement.

Aerosols generated from the above method were mixed with dry compressed air and were passed through a tube furnace where particles undergo oxidation in air for a given temperature (600–1100°C) and a residence time ( $\sim 1$  s). A 120 cm long quartz tube with 1 cm i.d. and a heated length of 30 cm was used as the reactor chamber. In the first set of experiments, these particles, following oxidation at different temperatures were sampled using electrostatic precipitation to a TEM grid (200 mesh nickel grid with silica film). Characterization was performed with a Zeiss EM10 TEM (accelerating voltage: 80 kV and magnification:  $100 \times$ – $200000 \times$ ).

A second set of experiments was aimed at measuring the inherent density of these oxidized nanoparticles and the experimental protocol was similar to our previous work by Park *et al.* [19]. In these experiments, particles were oxidized at different temperatures and were passed through a neutralizer to give them a Boltzmann charge distribution, and were then sent to a DMA [17], which selects particles all with the same mobility size. The DMA consists of two concentric cylinders, where aerosol is metered through a slit within the annular gap between the cylinders. An electric field is created by applying voltage to the inner cylinder while the outer cylinder is grounded. The electric force on the particle is balanced by the drag force, and at a fixed voltage, we obtain particles of same mobility size exiting the instrument. For this study, we looked at particles with a mobility size of 100 nm. The output stream of the DMA was sent to an Aerosol Particle Mass-Analyser APM [18, 19]. The APM consists of two concentric cylinders rotated at a controlled speed with the inner cylinder held at a high voltage creating an electric field within the annular region. Particles introduced in the annular region of the APM experience opposing electric and centrifugal forces such that all particles exiting the instrument have equivalent mass. These particles were then sampled onto a TEM grid using an eight-stage low-pressure impactor (LPI) [22] and were observed using the JEOL 1210 TEM (accelerating voltage: 40–120 kV, magnification:  $50 \times$ – $800000 \times$ ) to calculate their volume. Density can then be calculated using the relationship between mass

and particle volume. A more thorough description of the experimental protocol is detailed elsewhere [19]

#### 4. Experimental results

Figure 2 shows the morphology of the particles oxidized at different furnace temperatures. The first image [figure 2(a)] is of particles oxidized at 800°C, and we see that all the particles are agglomerates of solid spheres. As the oxidation temperature is increased to 900°C almost all the primary particles are still solid spheres. Increasing the oxidation temperature further, to 1000°C, however results in hollow spheres which can be seen in figure 2(c). Figure 2(d) is HRTEM micrograph of particles oxidized at these high temperatures and it clearly shows that the particles oxidized at these temperatures are hollow in nature. While not shown, all samples oxidized below 800°C, were found to be solid spheres, while particles oxidized at 1100°C (the highest temperature of our furnace) were found to be hollow.

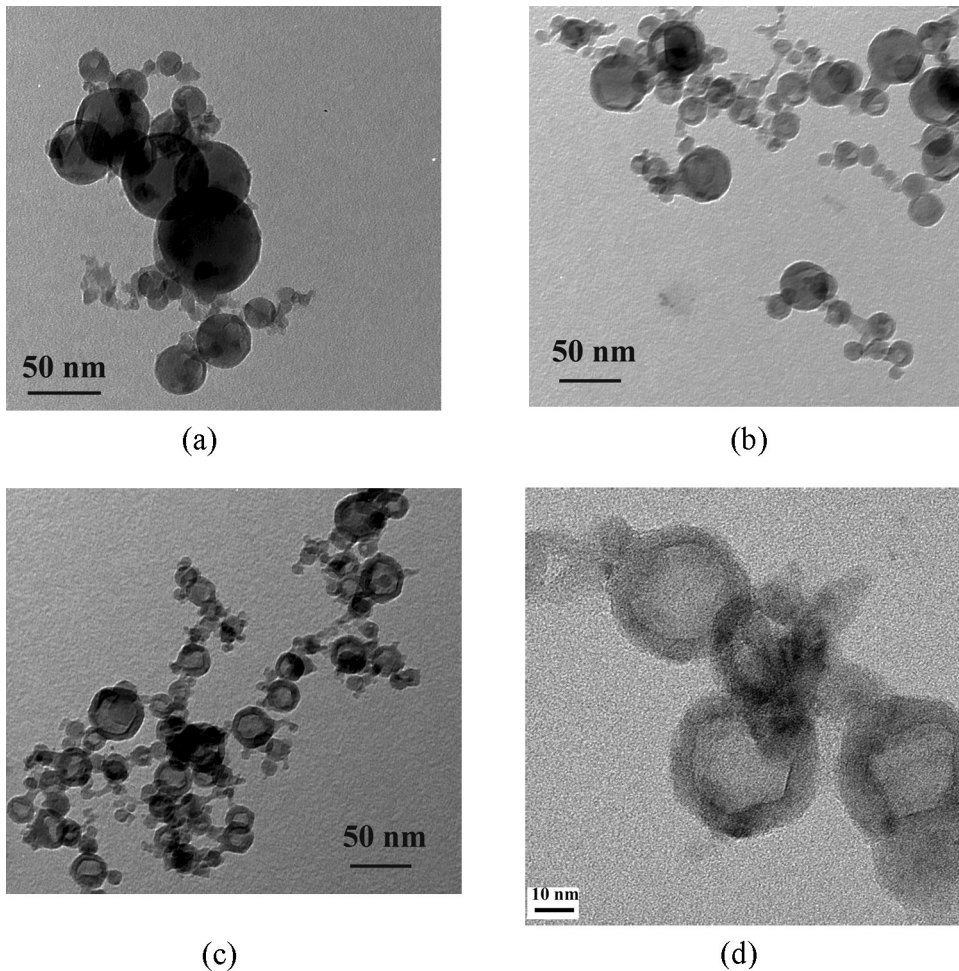


Figure 2. TEM micrographs of the aluminium particles oxidized at different temperatures: (a) 800°C, (b) 900°C, (c) 1000°C and (d) HRTEM of hollow particles after oxidation.

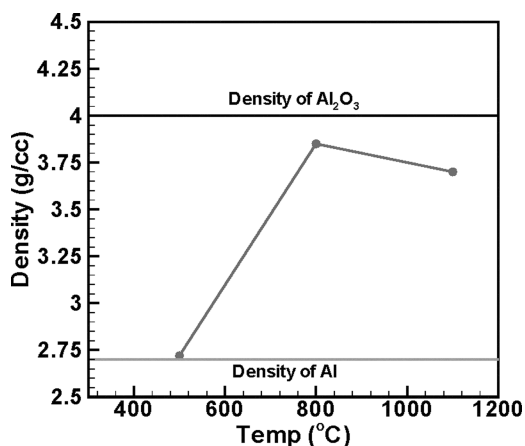


Figure 3. Measurement of inherent density of aluminium particles oxidized at different temperature.

Density measurements as described above were conducted at different oxidation temperatures and are shown in figure 3. We found that as we increase the furnace temperature from 500°C to 800°C, the density of the particles went up from 2.72 g/cc to 3.85 g/cc. Since the bulk density of aluminium is 2.7 g/cc, while that of bulk aluminium oxide is 4.0 g/cc, this increase in particle density corresponds essentially exactly to the conversion of aluminium to aluminium oxide, and is consistent with our prior mass-spectrometry results [16]. A further increase in temperature to 1100°C results in a drop of density, which we attributed to the presence of hollow particles, consistent with the TEM measurements.

## 5. Implication of the experimental measurements

The nominal expectation is that oxidation proceeds by the transport of the oxidizer through the oxide layer to the core, much like a shrinking core model. However the experimental observations clearly indicate the presence of particles with voids at temperatures higher than or equal to 1000°C. This suggests that the outward diffusion of aluminium may be the important phenomenon to describe the oxidation of aluminium nanoparticles at these temperatures. This argument is further substantiated by recent observations by Yin *et al.* on cobalt sulfide nanoparticles [23], who demonstrated the formation of hollow nanocrystals and suggested that the cavity in the particle forms from differences in diffusion rates between the two components. This justifies the argument that unlike a micron-sized particle, which burns in the vapour phase (drop burning model), oxidation of aluminium nanoparticles will involve more of a surface phenomenon, and subsequent transport through the oxide shell formed as a result of oxidation.

In our earlier work [15], we discussed the importance of phase change of aluminium on the oxidation of aluminium nanoparticles, and suggested that onset of oxidation coincides with the melting of aluminium (using commercially available nanoaluminium). This result was not in agreement with what other researchers [13] have observed using conventional thermal techniques, such as TGA and differential scanning calorimetry (DSC), where the onset of oxidation of aluminium was observed at around 550°C, and therefore lower than the melting point of aluminium.

The question of course is how to rationalize these differences. If we look at the above-mentioned observations, a significant difference between the oxidation experiment in the

aerosol phase (our work) and conventional thermal techniques is the time scale of the oxidation. In conventional thermal techniques, oxidation occurs over several minutes while our work in the aerosol phase is complete in under a second. In other words conventional thermal methods are probing physical chemical processes that are as much as three orders of magnitude slower. Our current belief is that the thermal methods are probing a slow oxidation process, which occurs below the melting point where the only mechanism for oxidation is the transport of the gas-phase oxidizer through the oxide shell to the aluminium core.

By contrast, in our experiment we observe the onset of oxidation above the melting point. Upon melting of aluminium, the density of aluminium changes from that of solid (2.7 g/cc) to a liquid (2.4 g/cc) resulting in an expansion of about 12%. But the expansion of the solid oxide shell is negligible and causes the oxide shell to be in tension and the aluminium metal core to be in compression. This pressure gradient present inside the particle can result in the rupture or thinning of the oxide shell [15, 24, 25] and thereby increasing the diffusion and hence the reaction rate. Also beyond the melting point, aluminium will be more mobile and is likely to diffuse outward. Furthermore, it should be expected that, because aluminium is a smaller ion, it should diffuse faster than oxygen and thus enhance the rate of oxidation. This is the fast oxidation regime that we observe in our experiments.

For oxidation temperatures beyond 1000°C, a drop in the density of the oxidized particles and the presence of hollow particles substantiates the fact that outward diffusion of aluminium is significant at these temperatures. Our morphological characterization and the density measurement suggests that hollow particles are observed only above 900°C and can be explained by considering simultaneous diffusion of aluminium and oxygen after the phase change of aluminium. It has been discussed earlier that a difference in the diffusion rates of the two components may result in formation of hollow particles [23]. We thus believe that although the diffusion of aluminium starts beyond the melting point, it becomes significant at these high temperatures and results in the formation of hollow particles.

Oxidation of aluminium nanoparticles can thus proceed in two distinct regimes. At temperatures below the melting point of aluminium, oxidation proceeds due to the diffusion of oxygen through the oxide shell, and it is the slow oxidation regime observed in conventional thermal techniques with longer residence time. But if the oxidation temperature is above the melting point of aluminium, it is the fast oxidation regime which we observe in our experiments, and in this regime the oxidation will proceed owing to melting of aluminium, rupture and thinning of oxide shell and diffusion of both aluminium and oxygen.

Finally the role of internal pressure on transport must be considered. With the core at high elevated pressure and the shell in tension (negative pressure), transport of the diffusing species will be affected by such steep gradients.

## 6. Model description

Based on our experimental observations we are now in a position to develop a model, that will capture the major issues addressed above and lead us to a better understanding of oxidation at the nanoscale.

As previously mentioned, micron-sized particles being much larger than the mean free path of air, burn with a boundary layer, and a flame stabilized around the particle (drop burning model). Metal evaporates from the particle surface, diffuses to the flame front, and undergoes a vapour phase combustion process. However, when we reach to the nano-length scale, these metal particles are smaller than the mean free path of air, and thus cannot sustain a diffusion flame and oxidation will involve surface chemistry and transport. The formation of the oxide layer implies that oxidation process will be governed by the diffusion of the reactants through

the oxide layer, and will not involve gas phase oxidation as that of a micron sized particle. That is not to say that a nanoparticle can never burn as a gas-phase process. If the gas temperature is sufficiently high then aluminium evaporation will lead to vapour phase aluminium burning and recondensation of the product as a new particle. That is however, not the problem being addressed. Our concern is the fate of an individual particle, not as an ensemble where the energy release per particle is not sufficient to raise the gas temperature.

There are other differences between micron and nanoaluminium which may be relevant and which must be accounted for in any credible model. It is well known that nanoparticles are at elevated pressures, as described by the Laplace–Young equation. However, recent molecular dynamics simulations [20] have shown that an oxide-coated aluminium nanoparticle has substantially high pressure gradients present inside the particle. Furthermore while the aluminium core will have positive pressure, the oxide shell is primarily under negative pressure (tension).

The model described here is based on the physics of the nanoparticle combustion as described above. It consists of a mass transfer model to describe the transport through the oxide layer, and an energy balance to account for the heat release during oxidation. It should be noted that the model described here does not consider the enhancement of reaction rate due to rupture or thinning of oxide shell, although the pressure gradients present inside the particle have been accounted for through the mass transfer model. Our earlier experimental work [16] has shown that the oxidation of aluminium nanoparticles is a transport controlled process, and the model developed here is based on this premise.

## 7. Nature of transport through the oxide layer

Based on our earlier experimental work [16], we have considered transport limited oxidation, and hence the intrinsic reaction rate is assumed to be infinite, and the transport flux of oxygen and aluminium inside the oxide shell determines the reacting flux. It is reasonable to assume that initially, the flux of oxygen reacting with the aluminium surface is equivalent to the collision rate in the free molecular regime. As the reaction proceeds, the oxide forms a coating on the particle following which both oxygen and aluminium may diffuse through this aluminium oxide coating.

As reported earlier, molecular dynamics simulations [20] have shown that there are significant pressure gradients present in the oxide shell. A natural effect of this pressure gradient will be the motion of atoms in the direction of decreasing pressure. This net transport of material in the direction of the gradient will be in addition to the diffusive transport within the oxide shell. It is thus reasonable to assume that the pressure gradient itself will result in a net velocity of atoms. If we define  $v_{\text{ox}}$  as the velocity of oxygen arising from this pressure gradient, and  $c$  as the concentration of oxygen in the oxide shell, then,  $cv_{\text{ox}}$  is the convective flux of oxygen due to the pressure gradient. Thus, the pressure effect can be thought of as an effective convective flux of oxygen and aluminium ions in addition to the diffusive flux due to concentration gradient. Particularly for small particles, this pressure gradient is quite significant [26], and may have a significant impact on the oxidation process. If  $D$  is the diffusion coefficient, we can write the oxygen flux,  $w_{\text{O}}$ , as

$$w_{\text{O}} = -D \frac{\partial c}{\partial r} + cv_{\text{ox}} \quad (1)$$

The phenomenological model for mass transport in the coated nanoparticle recently proposed by Dalla Torre *et al.* [27] for silicon has been extended here to describe the oxidation of aluminium nanoparticles with a pressure gradient present within the particle.

We can write the diffusion coefficient

$$D = k_B T \times \frac{v_{\text{ox}}}{(-\Delta P V_O)}$$

where  $\Delta P$  is the pressure gradient in the particle,  $V_O$  is the solubility volume of oxygen in aluminium oxide, taken to be  $0.02 \text{ nm}^3$  based on work of Dalla Torre *et al.* [27], and  $T$  is the temperature of particle. This relation can be thought of as an Einstein's relation for diffusion,  $D = k_B T \times \frac{v}{F}$ . In this particular case,  $(-\Delta P V_O)$  is the convective force acting on the moving species. If we define  $\gamma = \frac{v_{\text{ox}}}{D}$ , then we will have  $\gamma = -\frac{\Delta P V_O}{k_B T}$  and subsequently the species balance equation, including the pressure effect, based on mass balance using the flux described by equation (1) will be

$$\frac{\partial c}{\partial t} = D \left\{ \frac{\partial^2 c}{\partial r^2} + \frac{\partial c}{\partial r} \left[ \frac{2}{r} - \gamma \right] - \frac{2c\gamma}{r} \right\} \quad (2)$$

At each step, we consider steady state diffusion of both the species. Aluminium transport is given by a similar equation. Oxygen will diffuse from outer surface of the particle to the reaction surface, while aluminium will diffuse from the metal/metal oxide interface to the reaction surface. Since the process is assumed to be transport controlled, aluminium and oxygen concentrations at the reaction surface will be zero and the reaction front will be dynamic and can be located by using the stoichiometry of formation of aluminium oxide as shown in figure 4. Solution, with appropriate boundary conditions on the metal/metal oxide interface, the outer surface of particle, and the internal pressure gradient, will give us the concentration profiles of oxygen and aluminium, and thus the reaction rate and extent of conversion as a function of time.

## 8. Energy balance

Energy release from the aluminum/oxygen reaction requires that we simultaneously solve the energy equation. The global reaction liberates 1675 KJ of energy per mole of condensed

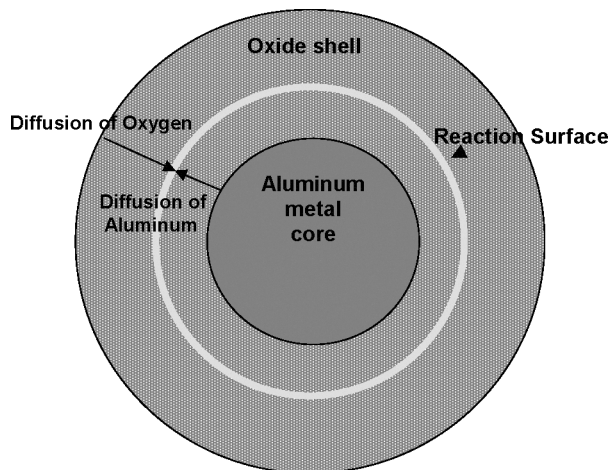


Figure 4. Schematic of an oxide-coated aluminium particle showing the metal core, oxide shell and the dynamic reaction surface.

product.



The energy balance, accounts for energy release from the reaction,  $q_{\text{gen}}$ , energy lost by conduction,  $q_{\text{cond}}$ , in the free molecule regime [28], energy used to heat the particle, and that used to evaporate aluminium from the particle,  $q_{\text{evap}}$  as follows.

$$q_{\text{gen}} = q_{\text{cond}} + q_{\text{evap}} + \frac{d}{dt}(m_p c_p T_p) \quad (4)$$

$$q_{\text{gen}} = 4\pi r^2 \times w_{\text{O}} \times \Delta h \quad (5)$$

$$q_{\text{cond}} = \frac{nv}{4} \times 4\pi R^2 \times 2k \times (T_p - T_{\text{air}}) \quad (6)$$

$$\frac{d}{dt}(m_p c_p T_p) = (m_{\text{Al}} c_{p_{\text{Al}}} + m_{\text{ox}} c_{p_{\text{ox}}}) \frac{dT_p}{dt} \quad (7)$$

Here  $n$  is the number of molecules per unit volume,  $v$  is the mean thermal speed of air molecules,  $k$  is the Boltzmann constant,  $T_p$  is the temperature of particle,  $T_{\text{air}}$  is the temperature of the surrounding air,  $r$  is the radius of reaction zone in the particle,  $R$  is the outer radius of the particle and  $w_{\text{O}}$  is the flux of oxygen reacting with aluminium at the reaction surface, which we obtain from the mass transfer models described above.  $m_{\text{Al}}$  and  $m_{\text{ox}}$  are the masses of aluminium and aluminium oxide in the particle, and  $c_p$  are their respective specific heats. In this model, particles are considered to be spherical and the aluminium oxide generated is assumed to form a spherical cap on the particle. The particle is assumed to be isothermal as conduction heat transfer within the particle will be fast relative to all other processes. At higher temperatures the vapour pressure of aluminium may cause significant evaporation, and result in evaporative cooling,  $q_{\text{evap}}$ , expressed as

$$q_{\text{evap}} = L_{\text{vap,Al}} \times w_{\text{Al}} \times 4\pi R^2 \quad (8)$$

Here  $L_{\text{vap,Al}}$  is the latent heat of vapourization of aluminium, and  $w_{\text{Al}}$  is the flux of aluminium evaporating from the surface of particle. The free molecular evaporation flux of aluminium is given by the following expression

$$w_{\text{Al}} = \frac{P_d}{\sqrt{2\pi R_g T M}} \quad (9)$$

Here  $R_g$  is the universal gas constant and  $M$  is the molecular mass of aluminum.  $P_d$  is the vapour pressure of aluminium just outside the drop, and is calculated using the Kelvin equation as follows:

$$P_d = P_0 \times \exp\left(\frac{4\sigma v_1}{k T d}\right) \quad (10)$$

$P_0$  is the vapour pressure of aluminium over a flat surface at temperature  $T$ ,  $\sigma$  is the surface tension of aluminium,  $v_1$  is the monomer volume which can be calculated using the bulk density of aluminium and  $d$  is the diameter of the drop. Vapour pressure and surface tension are calculated using the expressions given below [29].

$$P_0 = \exp\left(13.07 - \frac{36373}{T}\right) \text{ Atmospheres} \quad (11)$$

$$\sigma = 948 - 0.202T \text{ Dyne/cm} \quad (12)$$

Equations (1) to (12) are used to model the combustion process of the aluminium nanoparticle, and to calculate extent of oxidation of the particle.

## 9. Model prediction and discussion

As described, the transport model has been modified to account for the large pressures expected, based on molecular dynamic simulations [20]. Stress analysis revealed a large pressure gradient present within the particle, with the oxide shell under negative pressure and metal core having a positive pressure. Campbell *et al.* [20] have computed pressure profiles for a 20 nm diameter Al/Al<sub>2</sub>O<sub>3</sub> particle, and we have employed their results in a simplified pressure gradient profile in our model as depicted in figure 5. For all cases the pressure gradient is negative in the oxide near the core and positive near the outer edge. The shaded portion in figure 5 represents the region in the oxide shell with pressure gradients. If the coating thickness is less than 1 nm then the entire oxide shell will have a gradient, but if the oxide thickness has grown significantly (thickness > 1 nm), then the centre of the oxide shell is given a constant large negative pressure (~1–2 G Pa). The peak value of negative pressure in the oxide shell for a 20 nm diameter particle has been taken from Campbell *et al.* [20]. The pressure gradient for different particle sizes has been estimated by varying the peak value of negative pressure in the oxide shell inversely with the radius, an approximation based on the Laplace–Young equation [30].

This model assumes diffusion controlled oxidation based on our previous work [16]. Diffusion coefficients for oxygen and aluminium in aluminium oxide have been widely reported in the literature, but there are huge variations in the values. Extrapolation of Reed and Wuensch [31] expression for the diffusion coefficient of oxygen in aluminium oxide to 1200°C, gives a value of  $8.41 \times 10^{-27}$  m<sup>2</sup>/s. In contrast, Campbell *et al.* [20] reported a value of  $7.4 \times 10^{-9}$  m<sup>2</sup>/s for the diffusion coefficient of oxygen. Similarly for aluminium, Garcia-Mendez *et al.* [32] reported a diffusion coefficient of aluminium to be  $1.5 \times 10^{-19}$  m<sup>2</sup>/s at 500°C, while Campbell *et al.* [20] reported it to be  $1.2 \times 10^{-8}$  m<sup>2</sup>/s.

Given that the transport properties of aluminium and oxygen in aluminium oxide are integral to our model, the fact that the discrepancies in reported transport coefficients are so large that the results would be completely changed by the particular choice, and that we at this time have no reasonable basis for choosing one over the other. We have chosen to estimate the value of

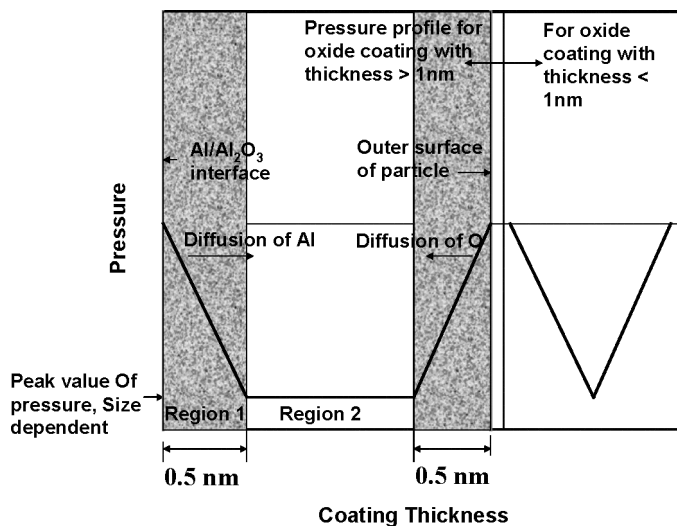


Figure 5. Pressure profile inside an oxide-coated aluminium particle. Left side of the figure shows the pressure profile for a particle having an oxide coating thickness greater than 1 nm while the right side is for particle with coating thickness less than 1 nm.

the diffusion coefficients by fitting the model results to those obtained experimentally from our aluminium oxidation experiments, to obtain an effective diffusion coefficient representing the net effect of the movement of both fuel and oxidizer through the oxide layer [16]. An Arrhenius fit to our data for particles less than 50 nm, gives  $D = 4.8691 \times 10^{-11} \exp(-4240.1/T)$  m<sup>2</sup>/s for the oxidizer in the temperature range of 600°C to 900°C. For this estimation, we assumed that the diffusion coefficient of aluminium ion is same as that of oxygen ion. This is relatively consistent with the work of Campbell *et al.* [20] who obtained a value of 1.6 using molecular dynamic simulation if we consider the fact that the variation of reported diffusion coefficients is over several orders of magnitude. We also need the solubility of oxygen and aluminium in aluminium oxide, which we were not able to find in the literature. For this work we assumed that the concentration of oxygen at outer surface of the particle is equivalent to that in the gas phase, and we used cobalt solubility in aluminium oxide reported in the literature [33] as the concentration of aluminium at the metal/metal oxide interface. We understand that these assumptions may result in errors in model predictions, but due to the unavailability of accurate data on physical properties, we found no reasonable alternative than to make these assumptions.

Figure 6 shows the extent of conversion, defined in terms of fraction of the volume of reacted aluminium as a function of reaction time. These calculations were done using the estimated diffusion coefficient in the model. Figure 6 shows the model predictions for different oxidation temperatures for an initially uncoated 20 nm radius particle having a residence time of 1 s in the reactor. Figure 6 also shows the data points for the experimentally determined extent of conversion for particles less than 50 nm at 1 s residence time from a previous study [16]. This result suggests that the estimated diffusion coefficient provides an acceptable fit to the experimental data. Also, the use of the estimated diffusion coefficient along with the assumptions stated above, results in capturing relatively quantitatively the temperature dependence, and the effective time scale for the overall oxidation process and also implies that the overall construct of the model is consistent with experimental observation.

One of the fundamental questions of interest is, how does the oxidation rate vary with particle size and why? Figure 7 shows the extent of conversion plotted against the reaction

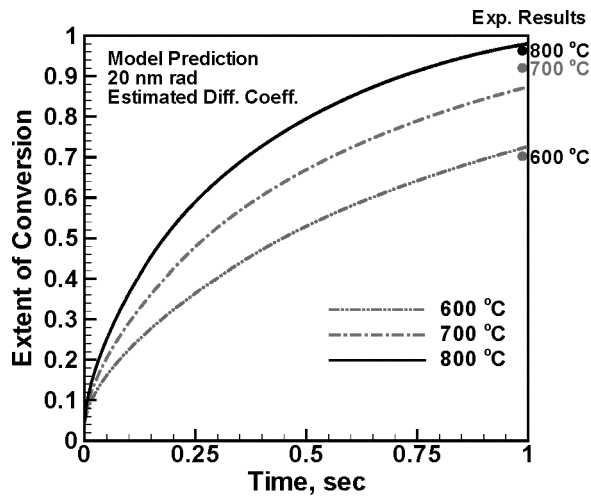


Figure 6. Extent of oxidation of a 20 nm particle at different temperatures using the estimated diffusion coefficient obtained from simulation with a pressure gradient of 2e18 Pa/m as suggested by molecular dynamic simulation [20]. A comparison with experimental results for residence time of 1 s [16] is also presented.

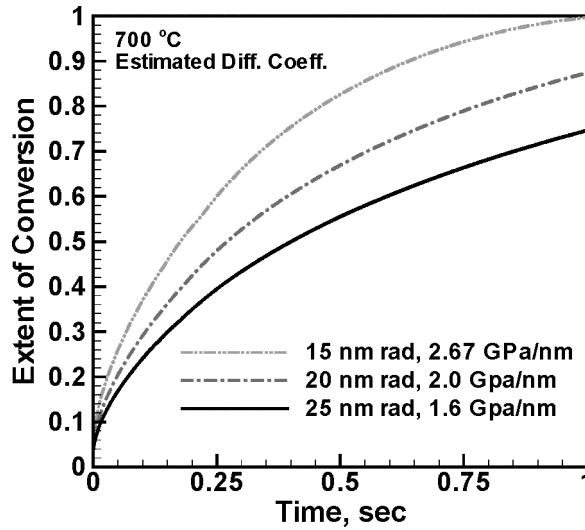


Figure 7. Extent of oxidation for particles of different sizes at 700°C using the estimated diffusion coefficient obtained by simulation and pressure gradients as listed in the legend.

time for particles of different size at 700°C. Not surprisingly as particle size decreases, the extent of oxidation goes up. As the particle size goes down, the surface area to volume ratio of the particle goes up, and this will increase the rate of any heterogeneous process, like a reaction controlled by diffusion. To understand this effect more clearly, we studied the variation of the time required to convert half the aluminium to aluminium oxide as a function of particle radius, and found a power law relation for the reaction time as shown in figure 8. By extension to different extents of conversions we find,  $t \propto r^{1.6 \pm 0.1}$ , where  $t$  is the time required for a particle to react to a certain extent and  $r$  is the initial radius of the particle. If this process was just a surface reaction in the free molecular regime, one should expect a linear relationship between

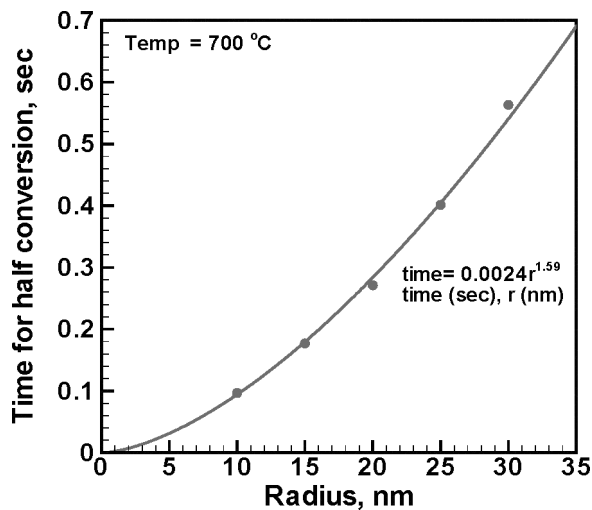


Figure 8. Variation of time taken for converting half of the particle by volume with the particle size fit to a power law.

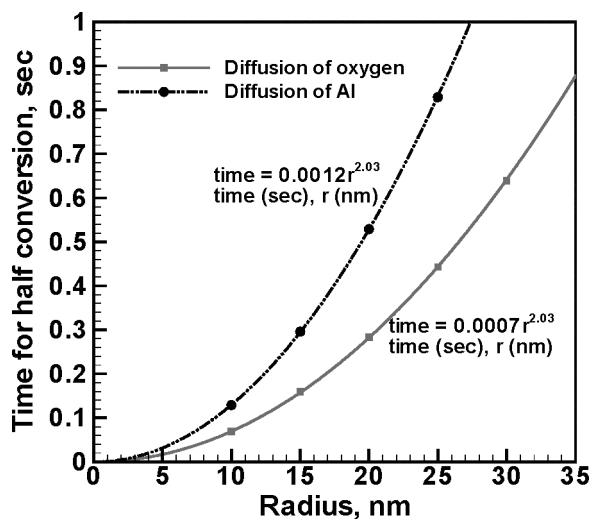


Figure 9. Time for 50% conversion as a function of particle radius, for either oxygen or aluminium diffusion (no pressure gradient effects included).

the time and radius. But here, diffusion of species through the aluminium oxide shell is the rate limiting step and hence it is not a purely surface process. If we have diffusion of either only aluminium or only oxygen through the oxide shell and without any pressure gradients, then the power law obtained is  $t \propto r^2$  as is shown in figure 9. This is in agreement with the shrinking core model [34] in the absence of pressure gradients. In these power law relations the large particle will take a longer time to react to the same extent of conversion as compared to a linear process. One reason is the fact that as the particle size is increased, to achieve a similar extent of conversion, the oxide shell thickness becomes large. The reactant species have to diffuse through this larger oxide shell and this reduces the reaction rate and thus we see the power law instead of a linear relationship. On considering diffusion of both species as suggested by the experimental observation along with the convective effect of the pressure gradient, we obtain a relation  $t \propto r^{1.6 \pm 0.1}$ , suggesting that the larger particles react faster than if we just considered a shrinking core model. This results in part because with both species diffusing towards each other, the effective diffusion length has been reduced since species are reacting within the shell. Of course this also means that larger particles are not quite so slow to react relative to smaller particles as might be expected from a simple shrinking core model. As such having two small particles, each half the volume of one large particle will give a characteristic reaction time that is a factor of 1.45 times faster for the same extent of conversion. Alternatively halving the particle diameter will increase the mass conversion rate by a factor of  $\sim 3$ .

Another important factor is the presence of increased pressure gradient in the smaller particles. To understand the effect of pressure gradient, we looked at variation of the normalized reaction rate with coating thickness at different values of the pressure gradient for a particle with an initial radius of 20 nm. These calculations are plotted in figure 10. For these calculations, the number of oxygen atoms reacting per unit time has been taken as a measure of reaction rate, which has been normalized with the reaction rate of a particle of radius 20 nm having a 2 nm coating in the absence of any pressure gradients. The first thing that can be clearly seen is that as the thickness of the oxide shell increases, the reaction rate decreases because the reacting species have to diffuse through a larger length. Understanding the effect of changing

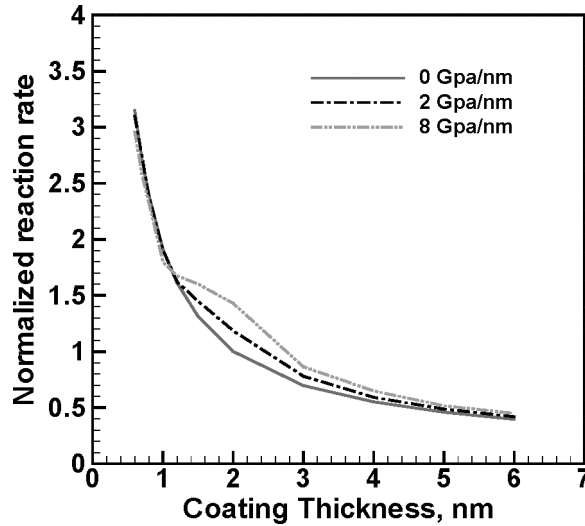


Figure 10. Normalized reaction rates versus coating thickness for different pressure gradients. Particle core radius = 20 nm;  $T = 700^{\circ}\text{C}$ .

pressure gradient requires knowledge of the position of the reaction surface at different coating thickness. As was said earlier, the reaction surface is dynamic in nature and is estimated by the stoichiometry for oxidation of aluminium. Coating thickness and the distance of reaction surface from the metal/metal oxide interface for the oxidation of a 20 nm particle at  $700^{\circ}\text{C}$  are plotted in figure 11. At the initial stages of oxidation, when the coating thickness is less than 1 nm, the reaction surface is at a distance much less than 0.5 nm from the metal/metal oxide interface, and thus in a region with a pressure gradient (figure 5). Oxygen has to diffuse in this region where the pressure gradient will act against the diffusion, and thus slows down

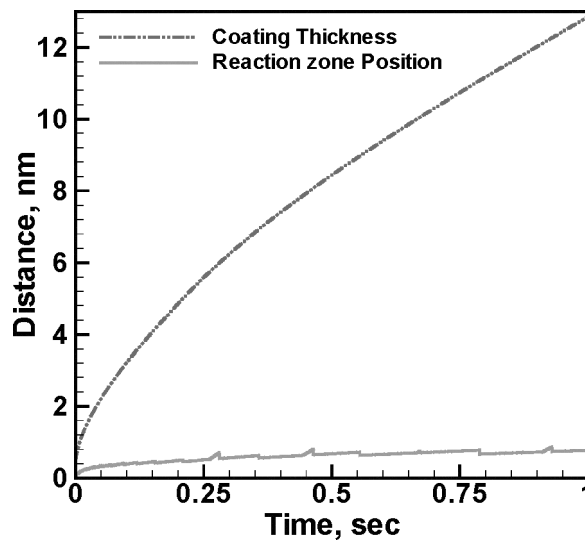


Figure 11. Coating thickness and distance of reaction zone from metal/metal oxide interface as a function of oxidation time. Initial radius = 20 nm;  $T = 700^{\circ}\text{C}$ .

the process. As a result, in the initial stages of oxidation, when the coating thickness is small, an increase in pressure gradient causes the oxidation rate to go down as can be seen in figure 10. When the coating thickness is in the range of 1–4 nm, the reaction surface is at a distance of about 0.5 nm from the metal/metal oxide interface. So both, aluminium and oxygen diffuse mostly in the region in which convection due to pressure gradient acts in the same direction as diffusion, and this enhances the rate of oxidation. Thus the pressure gradient increases the reaction rate when the thickness of the oxide shell is 1–4 nm. When the coating thickness increases further, the reaction zone moves further from metal/metal oxide interface. Here also both aluminium and oxygen diffuse in the region in which convection due to pressure gradient acts in the same direction as diffusion, and thus increases the reaction rate. However, as can be seen in figure 10, this effect gets attenuated when the coating thickness is large, and the reason for this is that the species also have to diffuse through a large region (figure 5) without any pressure gradient. Thus we see that at different stages of oxidation the pressure gradient acts in different ways, and this can result in the time–radius relationship that we have estimated.

## 10. Conclusions

Experimental studies were conducted to study the morphology of the aluminium particles oxidized at different temperatures. At temperatures 1000°C or higher, we observed that particles are hollow. This fact was further substantiated by the measurement of density of these particles using DMA [17] and APM [18, 19]. It was found that as we increased the oxidation temperature from 500°C to 800°C, density of particles increased from 2.72 g/cc to 3.85 g/cc indicating the conversion of particles from aluminium to aluminium oxide. However, as we increase the temperature further to 1100°C, the density again drops indicating the presence of hollow particles. On the basis of these experimental observations, our prior experimental observations [15, 16], along with those available in literature [13, 24, 25], it was concluded that the oxidation of aluminium can proceed in two regimes. At temperatures below the melting point, we have a slow oxidation regime in which the primary mechanism of oxidation is the diffusion of oxygen through the oxide shell. Above the melting point of aluminium, we have the fast oxidation regime with diffusion of both aluminium and oxygen, which may be enhanced by rupture and thinning of oxide shell, and is consistent with the formation of hollow particles.

We also developed a phenomenological model to describe the oxidation of aluminium nanoparticles, which incorporates data from experimental results [16] and molecular dynamics simulation [20] to interpret and explain the oxidation process. This model incorporates the effect of the large pressure gradients present in these particles which can affect the oxidation process. We found a power law relation ( $t \propto r^{1.6 \pm 0.1}$ ) between the reaction time and particle size. This power law relation suggests that the larger particles will react faster than what is predicted by a simple shrinking core model ( $t \propto r^2$ ) and we attribute this to the fact that both the reacting species are diffusing in the oxide shell which reduces the effective diffusion length.

## Acknowledgement

This work is supported by the ARMY-DURINT Center for NanoEnergetics Research.

## References

- [1] Brzustowski, T.A. and Glassman I., 1964. In: H. G. Wolfhard, I. Glassman, and L. Green Jr. (Eds), *Heterogeneous Combustion* (New York: Academic Press), p. 41.

- [2] Law, C.K., 1973, *Combustion Science and Technology*, **7**, 197–212.
- [3] Brooks, K.P. and Beckstead, M. W., 1995, *Journal of Propulsion Power*, **11**, 769–780.
- [4] Widener, J.F. and Beckstead, M.W., 1998, *Aluminium Combustion Modeling in Solid Propellant Combustion Products*, AIAA 98–3824.
- [5] Liang, Y. and Beckstead, M.W., 1998, *Numerical Simulation of Quasi-Steady, Single Aluminium Particle Combustion in Air*, AIAA 98-0254.
- [6] Liang, Y. and Beckstead, M.W., 1997, 34th JANAF Meeting 4, pp. 197–208.
- [7] Liang, Y. and Beckstead, M.W., 1998, *Numerical Simulation of Unsteady, Single Aluminium Particle Combustion in Air*, AIAA 98-3825.
- [8] Widener, J.F., Liang, Y. and Beckstead, M.W., 1998, 35th JANAF Meeting 1, pp. 577–592.
- [9] Ernst, L.F., Dryer, F.L., Yetter, R.A., Parr, T.P. and Hanson-Parr, D.M., 2000, *Proceedings of the Combustion Institute*, 871–878.
- [10] Bucher, P., Ernst, L., Dryer, F.L., Yetter, R.A., Parr, T.P. and Hanson-Parr, D.M., 2000, *Progress in Astronautics and Aeronautics*, 689–722.
- [11] Trunov, M.A., Schoenitz, M., Zhu, X. and Dreizin, E.L., 2005, *Combustion and Flame*, **140**, 310–318.
- [12] Ivanov, G.V. and Tepper, F., 1997. In: K. K. Kuo (Ed.), *Fourth International Symposium on Special Topics in Chemical Propulsion*, p. 636.
- [13] Mench, M.M., Kuo, K.K., Yeh, C.L. and Lu, Y.C., 1998, *Combustion Science Technology*, **135**, 269–292.
- [14] Aumann, C.E., Skofronick, G.L. and Martin, J.A., 1995, *Journal of Vacuum Science Technology*, **B13**, 1178–1183.
- [15] Rai, A., Lee, D., Park, K. and Zachariah, M.R., 2004, *Journal of Physical Chemistry*, **B108**, 14793–14795.
- [16] Park, K., Lee, D., Rai, A., Mukherjee, D. and Zachariah, M. R., 2005, *Journal of Physical Chemistry*, **B109**, 7290–7299.
- [17] Knutson, E.O. and Whitby, E.R., 1975, *Journal of Aerosol Science*, **6**, 443–451.
- [18] Ehara, K., Hagwood, C. and Coakley, K.J., 1996, *Journal of Aerosol Science*, **27**, 217–234.
- [19] Park, K., Kittelson, D.B., Zachariah M.R. and McMurry, P.H., 2004, *Journal of Nanoparticle Research*, **6**, 267–272.
- [20] Campbell, T., Kalia, R.K., Nakano, A., Vashishta, P., Ogata, S. and Rodgers, S., 1999, *Physical Review Letters*, **82**, 4866–4869.
- [21] Park, K., Rai, A. and Zachariah, M.R., 2006, *Journal of Nanoparticle Research*, **8**, 455–464.
- [22] Hering, S.V., Friedlander, S.K., Collins, J.J. and Richards, L.W., 1979, *Environment Science and Technology*, **13**, 184–188.
- [23] Yin, Y., Rioux, R.M., Erdonmez, C.K., Hughes, S., Samorjai, G.A. and Alivisatos, A.P., 2004, *Science*, **304**, 711–714.
- [24] Storaska, G.A. and Howe, J.M., 2004, *Material Science Engineering*, **A368**, 183–190.
- [25] Rosenband, V., 2004, *Combustion and Flame*, **137**, 366–375.
- [26] Hawa, T. and Zachariah, M.R., 2004, *Journal of Chemical Physics*, **121**, 9043–9049.
- [27] Dalla Torre, J., Bocquet, J.L., Limoge, Y., Crocombette, J.P., Adam, E., Martin, G., Baron, T., Rivallin, P. and Mur, P., 2002, *Journal of Applied Physics*, **92**, 1084–1094.
- [28] Loyalka, S. and Williams, M.M.R., 1991, *Aerosol Science: Theory and Practice: with Special Application to the Nuclear Industry* (New York: Oxford Publishers).
- [29] Panda, S. and Pratsinis, S.E., 1995, *Nanostructured Materials*, **5**, 755–767.
- [30] Zhang, C.Y., Wang, C.X., Yang, Y.H. and Yang, G.W., 2004, *Journal of Physical Chemistry*, **B108**, 2589–2593.
- [31] Reed, D.J. and Wuensch, B.J., 1980, *Journal of The American Ceramic Society*, **63**, 88–92.
- [32] Garcia-Mendez, M., Valles-Villarreal, N., Hirata-Flores, G.A. and Farias, M.H., 1999, *Applied Surface Science*, **151**, 139–147.
- [33] Gontier-Moya, E.G., Erdelyi, G., Moya F. and Freitag, K., 2001, *Philosophical Magazine*, **A81**, 2665–2673.
- [34] Levenspiel, O., 1999, *Chemical Reaction Engineering*, 3rd edition (New York: John Wiley).